PROCEEDINGS, Thirty-Sixth Workshop on Geothermal Reservoir Engineering
Stanford University, Stanford, California, January 31 - February 2, 2011
SGP-TR-191

A STUDY OF NUMERICAL SIMULATIONS OF MIXED-MODE FRACTURE PROPAGATION IN ROCK

K.S. Min, K. Huang, A. Ghassemi

Harold Vance Department of Petroleum Engineering, Texas A&M University,
3116 TAMU College Station, TX 77840, USA
e-mail: ahmad.ghassemi@pe.tamu.edu

ABSTRACT

Fracture propagation, especially for fractures emanating from inclined wellbores and closed natural fracture often involves Mode I, Mode II and at times Mode III fracture pattern. When an embedded inclined 3D fracture is subjected to compression, the fracture tips are restrained by the surrounding materials so that it does not propagates as predicted by 2D fracture models. In this paper, three-dimensional mixed-mode fracture growth from an initially embedded circular crack is studied using two numerical approaches. The virtual multidimensional internal bond (VMIB) and damage mechanics have been implemented within a finite element method along with an element partition algorithm (EPM) to simulate 3D crack growth. The VMIB approach has been utilized to simulate multiple cracks. The damage approach has shown to be effective when considering rock heterogeneity and thermal stresses and thus is also considered in this work.

INTRODUCTION

Simulation of 3D fracture propagation is complex as it often simultaneously involves all three fracture modes over a contour. Whereas in 2D case the zone of interest is only a point (fracture tips), in 3-D case the fracture tip is a closed boundary making it difficult to develop a fracture criterion for predicting propagation at different points along its edge as each point has a different stress intensity factor. Another major challenge in modeling fracture propagation using the linear elastic finite element method is the need for remeshing as the fracture propagates. Lazarus (Lazarus 2003) has theoretically studied the 3D fracture propagation subjected to uniform remote tensile loading and concluded that a closed crack tends to propagate to become circular and that for the material of heterogeneous toughness, the crack tends to propagate to ensure that the stress intensity factor reaches the toughness along the whole front.. Because of the strong discontinuity of cracks and the heterogeneous nature of rock, it is very difficult to numerically replicate 3D crack paths. Currently, a number of techniques are used to simulate crack growth including boundary element, finite elements and the discrete element methods. The latter (DEM) uses the interaction behavior between particles used to represent the discontinuous aspect of the solid. However, DEM requires numerous particles in order to represent realistic problem geometry and accuracy, resulting in a high computational cost. Also, it is very difficult to model realistic particle geometries and to determine the material parameters required in defining mechanical relationship between these “micro-scale” particles, causing significant errors during simulation. Alternative include the Virtual Internal Bond (VIB) method or damage mechanics. The VMIB model has been proposed to bridge the processes micro bond rupture and macro fracture (Zhang and Ge 2005). The three-dimensional constitutive relation of VMIB is derived from the one-dimensional bond in the micro scale and is implemented in a 3D finite element method. To represent the contact and friction between fracture faces, the three-dimensional element partition method is employed.

Damage evolution law with Mohr-Coulomb failure criterion has been used to model large scale stimulation (Lee and Ghassemi 2010). It can also be used in a 3D FEM with element partition methodology to represent brittle failure of rock and fracturing. The advantage of this method is that elements are not deleted during fracture propagation and mass of the system if preserved. An element partitioning algorithm similar to the one used in VMIB provides for flexible crack patterns during simulation. Most fractures in rock have strong internal heterogeneity, lateral variability and non-planar geometry. Statistical models of heterogeneity can account for a variety of possibilities, so that Weibull distribution function is applied within the damage approach.

3D FRACTURE PROPAGATION SIMULATION IN ROCK USING THE VMIB

The model is applied to simulate fracture propagation and coalescence in typical laboratory experiments, and to analyze the propagation on an embedded fracture. The case studies include fractures subjected to tensile and compressive loads. Also, mixed-mode propagating embedded fracture is considered. In addition, a procedure for application of fluid pressure is developed and used to simulate hydraulic fracturing.

In the VMIB method, the solid is considered as randomized material particles at the micro scale. A macro constitutive relation is then derived from the cohesive law between material particles, which makes the separate fracture criterion unnecessary. Zhang and Ghassemi (Zhang and Ghassemi 2010) and Min et al (Min et al. 2010) have accounted for poroelasticity and heterogeneity. Also, by considering the shear effect, the VMIB can account for different values of Poisson's ratio, therefore, it can be applied to wider range of engineering materials. The VIB (Gao and Klein 1998; Klein and Gao 1998) considers the solid to consist of randomized material particles on the micro scale (Fig.1a). The material particles interact with virtual internal bonds, as shown in Fig.1b. The virtual bond has both normal and shear stiffness. When the bond is linear elastic, the derived constitutive relation is:

$$\mathbf{C}_{ijkl} = \int_0^{2\pi}\int_0^{\pi} f(\varepsilon)\left[k\xi_i\xi_j\xi_k\xi_l + r\xi_i\boldsymbol{\eta}'_j\xi_k\boldsymbol{\eta}'_l + r\xi_i\boldsymbol{\eta}''_j\xi_k\boldsymbol{\eta}''_l + r\xi_i\boldsymbol{\eta}'''_j\xi_k\boldsymbol{\eta}'''_l\right] D(\theta,\phi)\sin(\theta)d\theta d\phi \quad (1)$$

where $\mathbf{C}_{ijkl}$ is the four-order elastic tensor, defined as $\boldsymbol{\sigma}_{ij} = \mathbf{C}_{ijkl}\boldsymbol{\varepsilon}_{kl}$; k, r are respectively the normal and shear stiffness of bond; $\boldsymbol{\xi}$ is the unit orientation vector of bond, $\boldsymbol{\xi} = (\sin\theta\cos\phi,\ \sin\theta\sin\phi,\ \cos\theta)$ in the sphere coordinate system; $\boldsymbol{\eta}$ is the orientation vector perpendicular to $\boldsymbol{\xi}$, $\boldsymbol{\eta}' = \boldsymbol{\xi}\times(\bar{\mathbf{x}}_1\times\boldsymbol{\xi})$, $\boldsymbol{\eta}'' = \boldsymbol{\xi}\times(\bar{\mathbf{x}}_2\times\boldsymbol{\xi})$, $\boldsymbol{\eta}''' = \boldsymbol{\xi}\times(\bar{\mathbf{x}}_3\times\boldsymbol{\xi})$, $\bar{\mathbf{x}}_i$ is the unit orientation vector of x_i axes. $D(\theta,\phi)$ is the bond density function, for simplification purpose, let $D(\theta,\phi)=1$ without loss of generality. $f(\varepsilon)$ is the bond evolution function:

$$f(\boldsymbol{\varepsilon}) = \exp\left[-c\left(\frac{|\boldsymbol{\xi}^T\boldsymbol{\varepsilon}\boldsymbol{\xi}|}{\varepsilon_b}\right)^n\right]\cdot\exp\left[-c\left(\frac{\boldsymbol{\xi}^T\boldsymbol{\varepsilon}^T\boldsymbol{\varepsilon}\boldsymbol{\xi}-(\boldsymbol{\xi}^T\boldsymbol{\varepsilon}\boldsymbol{\xi})^2}{\varepsilon_b^2}\right)^n\right] \quad (2)$$

where ε_b is a micro coefficient, $\varepsilon_b = \varepsilon_t$ if $\boldsymbol{\xi}^T\boldsymbol{\varepsilon}\boldsymbol{\xi} \ge 0$ whereas $\varepsilon_b = \varepsilon_c$ if $\boldsymbol{\xi}^T\boldsymbol{\varepsilon}\boldsymbol{\xi} < 0$ with ε_t and ε_c respectively being the strain at the peak stress in uniaxial tensile and compressive test; c, n are the shape coefficients which determine the shape of stress-strain curve. The term $\boldsymbol{\xi}^T\boldsymbol{\varepsilon}\boldsymbol{\xi}$ in Eq.(3) means the relative normal deformation of bond and the term $\boldsymbol{\xi}^T\boldsymbol{\varepsilon}^T\boldsymbol{\varepsilon}\boldsymbol{\xi} - (\boldsymbol{\xi}^T\boldsymbol{\varepsilon}\boldsymbol{\xi})^2$ means the relative shear deformation of bond. The relationship between the micro constants (k,r) and the macro constants (E,ν) is

$$k = \frac{3E}{4\pi(1-2\nu)}, \qquad r = \frac{3E(1-4\nu)}{4\pi(1+\nu)(1-2\nu)} \quad (3)$$

where E and ν are respectively the Young's modulus and Poisson ratio.

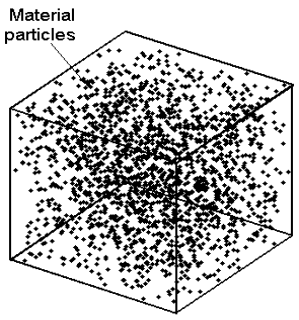

(a)

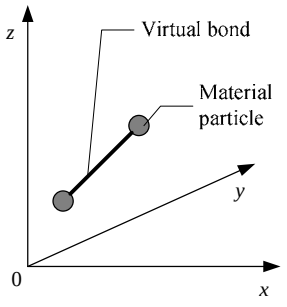

(b)

Fig.1 Material constitution in micro scale from the view of VIB: (a) the randomized material particles and (b) material particles are bonded with virtual bond.

3D ELEMENT PARTITION METHOD

One of the challenges for 3D fracture simulation is the representation of pre-existing cracks and newly extended crack surfaces. 3D element partition method (3D EPM) is used to describe the contact and friction between the fracture surfaces which subjected to the compressive stress. The 3D EPM take advantage of

the geometry features of tetrahedron element to construct a four-node contact element. When a fracture cuts through a tetrahedron element, two types of four-node contact element, i.e. Type I and Type II, are formed.

SIMULATION EXAMPLES

To examine the performance in simulating tensile fractures (Mode I fracture) propagation and their interaction, a specimen with two sawed horizontal rectangular fracture is simulated. The geometry and boundary conditions are shown in Fig. 3. Table.1 shows the parameters used. The mesh consist of 12 rows of nodes plotted on the x-direction, 24 rows nodes plotted on the y-direction, and 34 rows nodes plotted on the z-direction. The total element number is $11\times23\times33\times5=41745$ and the total node number is $12\times24\times34=9792$. Displacement controlled load is used in this simulation. Each step is given by $\Delta d=0.025\times\varepsilon_t\times1=2.62\times10^{-3}mm$ .Total step is 120.

Table 1: Simulation parameters

Parameters of intact element		Parameters of 3D EPM		Parameters of 3D VMIB	
E (GPa)	30.5	K_n(GPa)	1.0	c	0.15
ν	0.20	K_s(GPa)	10^{-8}	n	4.0
ε_t (10^{-3})	0.105	h (mm)	1.0		

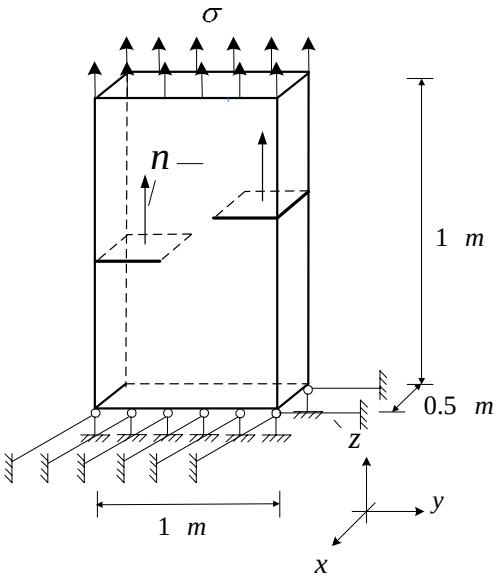

Fig.2 Dimensions and boundary condition of cubic specimen with two sawed horizontal rectangular fracture.

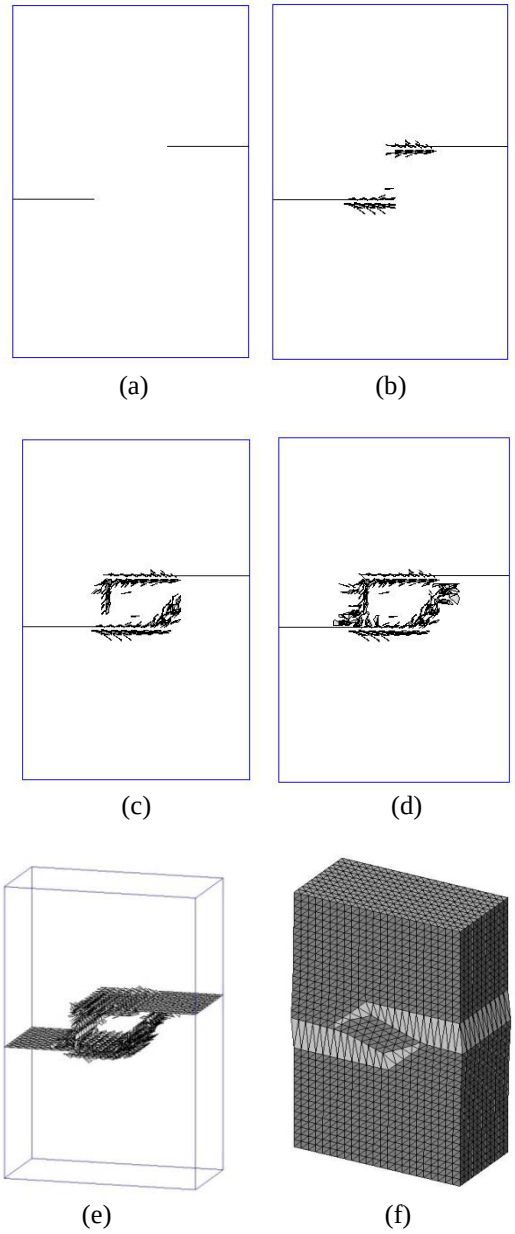

Fig.3 Fracture propagation progress: (a) initial fracture; (b)~(d) fracture propagation; (e) fracture surface at failure; (f) deformed mesh configuration (node displacements magnified 300 times).

Fig.3 (a) shows the initial and final fracture patterns. From Fig. 3(b) to (d), the fractures develops from initial crack tips and propagate horizontally as a typical Mode I fracture. Due to the existing of other fracture, the stress field around the fracture tip is disturbed. Consequently, the newly extend fracture deviates along the direction towards the other one and converge at the end. Fig. 3(e), (f) shows the fracture surface and deformed mesh configuration at failure upon specimen failure.

The second simulation explores Mode II fracture propagation and interaction. A specimen with two sawed inclined rectangular fracture is simulated. The dimensions and boundary conditions are shown as Fig. 4. Material and model parameters showed in Table.1. In present meshing scheme, there are 26 rows of nodes plotted on the x direction, 26 rows nodes plotted on the y direction, and 26 rows nodes plotted on the z direction. The total element number is $25\times25\times25\times5=78125$ and the total node number is $26\times26\times26=17576$. Displacement controlled load is used in this simulation. Each step is $\Delta d=0.002\times\varepsilon_t\times1=0.0209\times10^{-3}mm$. Total step is 120. Fig. 6(a) shows the initial fracture.

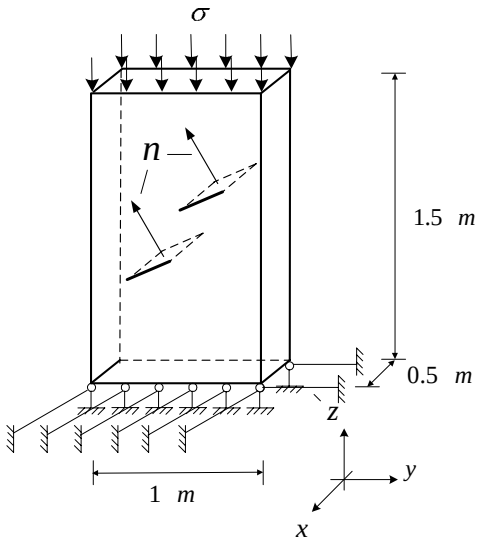

Fig.4 Dimensions and boundary condition of cubic specimen with two sawed inclined rectangular fracture.

From Fig. 5(b) to (d), the fractures propagate from both wings of the initial cracks. The left wing of lower initial fracture and the right wing of upper fracture yield newly-extended fracture firstly along the direction perpendicular to the fracture surface. Then, the newly extended fractures develop along the vertical direction of the specimen. This phenomenon is well agrees with that in the experiment. The fractures derive from near side initial fracture tips converge in the middle of the specimen. Fig. 5(e), (f) shows the fracture surface and deformed mesh configuration at failure. This agrees with experimental observations in Fig 6 (Bobet and Einstein 1998).

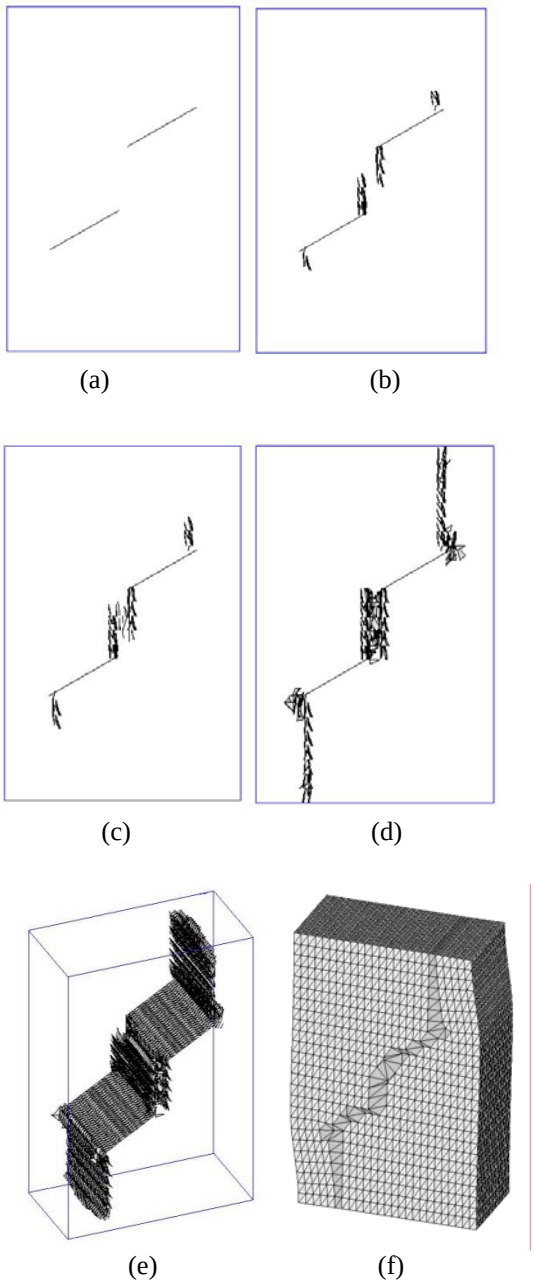

Fig.5 Fracture propagation progress: (a) initial fracture; (b)~(d) fracture propagation; (e) fracture surface at failure;(f) deformed mesh configuration (node displacements magnified 300 times).

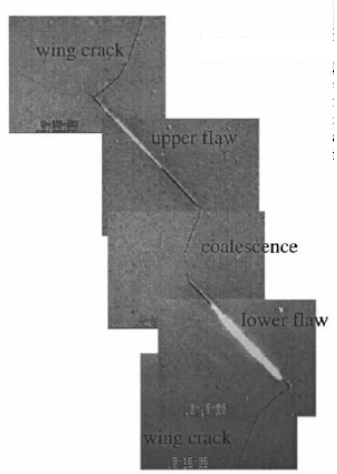

Fig. 6 Experiment of wing crack growth in uniaxial compression by (Bobet and Einstein 1998).

Modeling Embedded fracture (Mix Mode-I, II-III)

Simulating the propagation of an embedded fracture subjected to shear stresses is a challenging problem in geomechanics. In this case, the fracture simultaneously evolves in Modes I, II and III. To model this phenomenon, consider the simulation of embedded elliptical fracture. The dimensions and boundary conditions are shown as Fig. 7. Material and model parameters showed in Table.1. In present meshing scheme, there are 32 rows of nodes plotted on the x direction, 32 rows nodes plotted on the y direction, and 32 rows nodes plotted on the z direction. The total element number is $31\times31\times31\times5=148955$ and the total node number is $32\times32\times32=32768$. Each step is $\Delta d=0.005\times\varepsilon_t\times1=0.0524\times10^{-3}mm$. Total step is 210. Fig. 8(a) shows the initial fracture.

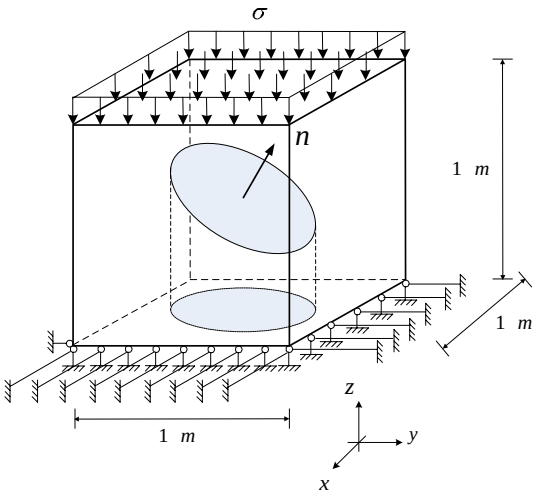

Fig.7 Dimensions and boundary condition of cubic specimen embedded with an elliptical fracture.

Fig. 8 shows that the fracture develops from upper and lower tips of initial fracture in a typical Mode II fracture. The fracture propagation is slower on the sides of the tip as it propagates outwardly to the lateral side of specimen. From Fig. 8, the side fracture that initiated from the side tip rotates from the initial crack tip toward the lateral side of specimen, which represents the Mode III response. This pattern of fracture propagation has been observed in experimental modeling of 3-D crack growth from pre-existing circular crack Adams and Sines (Adams and Sines 1978). Also, Dyskin et al (Dyskin AV 2003) tested wing crack model using a brittle material including the presence of the contact effect at 2003. In their experiments, Dyskin et al. observed secondary cracks (called "wings") branched towards the axis of compression from the upper and lower tips of the initial circular crack due to mixed mode of $\mathbf{K}_{II}$ and $\mathbf{K}_{III}$ related to the contact between pre-existing crack surface (Fig 9, 10.)

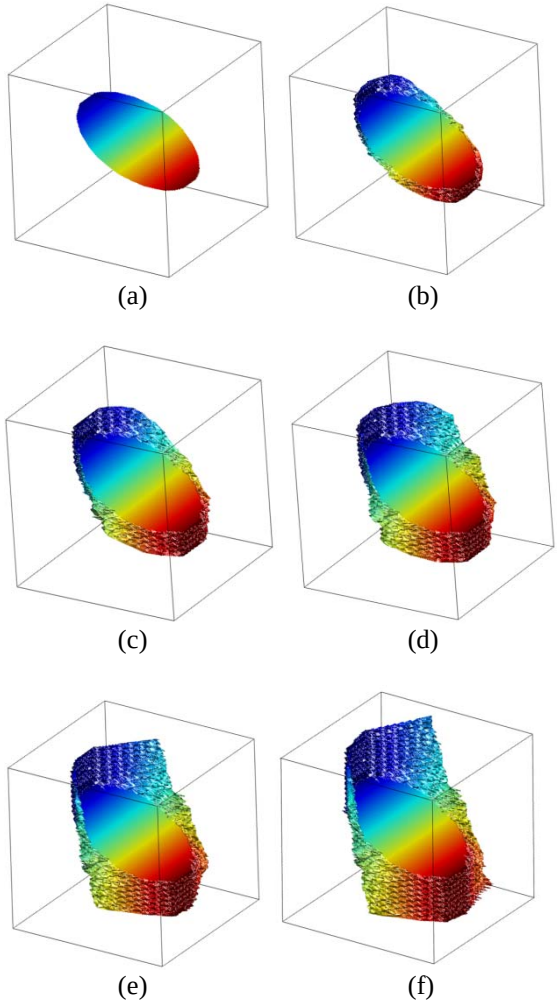

Fig.8 Fracture propagation progress: (a) initial fracture; (b)~(f) fracture propagation.

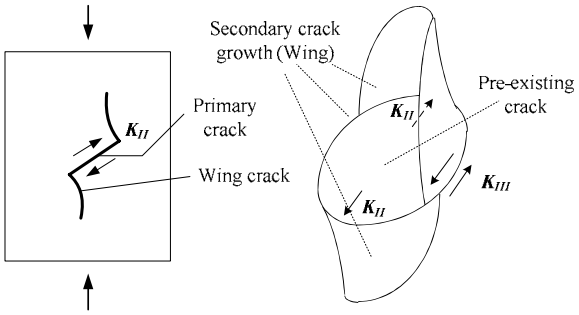

Fig.9 2D wing crack growth (K_{II}) and 3D wing crack growth (Mixed mode of K_{II} &K_{III}).

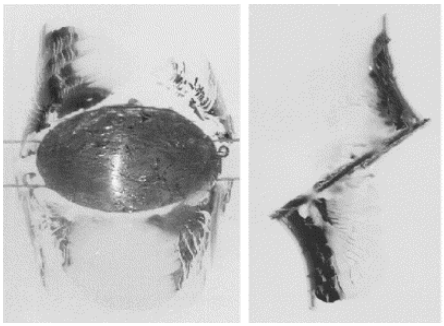

Fig.10 Fragment of a resin sample with a sing wing crack. (two horizontal lines are threads holding the inclusion) from experimental results of Dyskin et al (Dyskin AV 2003).

HYDRAULIC FRACTURE SIMULATION

For the purpose of hydraulic fracturing simulation, consider the interaction of clusters of minifracs that have been initiated through perforations or in openhole completions in deviated wells (wells that are not parallel to a principal stress direction). A horizontal wellbore with three transverse three parallel fractures is shown in Fig. 11. The normal directions of natures fracture are parallel to wellbore. The fluid is pumped into fractures and causes the hydraulic fracturing. The wellbore is relative small compared with the nature fracture, so the influence of wellbore is neglected. Table 1 lists the parameters used in all simulation in the present report. In present meshing scheme, there are 30 rows of nodes plotted on the x direction, 44 rows nodes plotted on the y direction, and 30 rows nodes plotted on the z direction. The total element number is $29\times29\times43\times5=180815$ and the total node number is $30\times30\times44=39600$. Each step is $\Delta pressure=75\times1000=7.5\times10^4\ N/m^2$. Total step is 142.

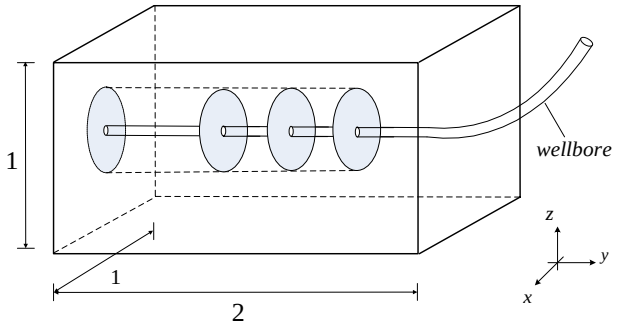

Fig. 11 Dimension of horizontal wellbore and the initial fractures

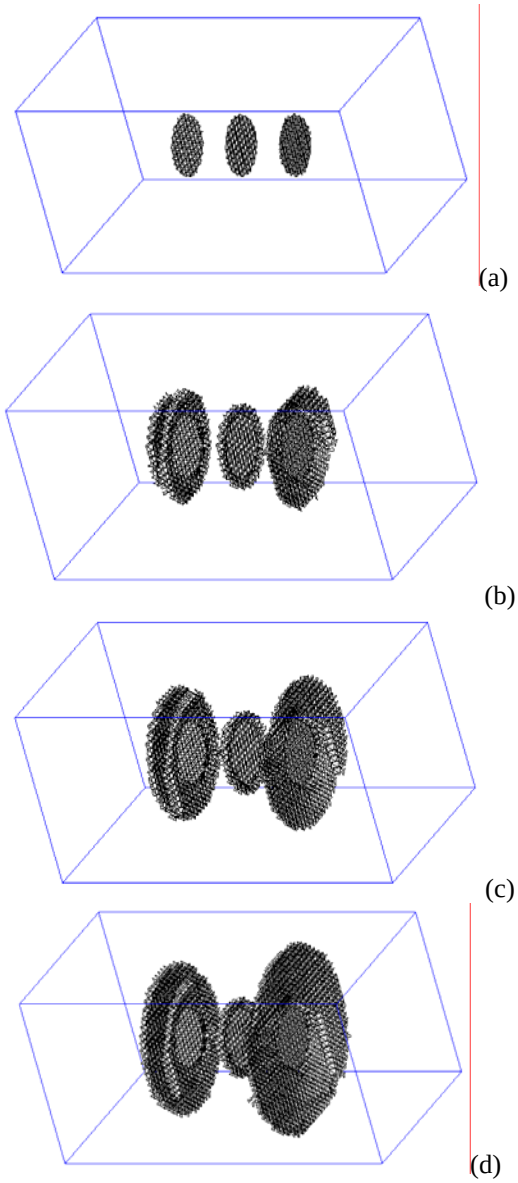

Fig. 12 Simulated hydraulic fracture propagation paths.

Fig. 12(a) shows the initial fracture configuration and subsequent propagation steps. It can be seen that fractures develop from the tip of each but the exterior fractures propagate faster compare with the middle one. That is because pressure on the middle fracture surface is offset by the pressure on the side ones. In another words, the middle fracture is confined by the pressure in the side fractures. So the fracture opening mainly occurs at the side facture, which along the original fracture direction. After pressure applied on the fracture surface reach a certain value, compressive failure occurs between the fractures due to the pressure compress the material between the adjacent fracture surfaces.

The simulation of propagation processes of hydraulic fracturing agree with analytical/numerical results and experimental observations. However, additional studies are needed to refine the model to effectively model larger scale problems. In particular, element size sensitivity must be reduced. This can be done based on the J-integral and cohesive zone theory and relating the bond evolution function to the critical J-integral and element size.

3D SIMULATION OF FRACTURE PROPAGATION USING A SYNTHETIC ROCK MODEL AND DAMAGE MECHANICS

Failure of brittle material is believed to involve growth of micro-cracks due to the interaction of material inhomogeneities and applied stresses. Coalesce of these microcracks leads to macroscopic material damaged zone expansion as microcrack population and intensity increases. The initiation and growth of damage can be described using Continuum Damage Mechanics (CDM). In this way, the material state can be macroscopically characterized using damage evolution laws. Also, it is recognized that crack path is initiated and propagates though severely damaged zone. Usually, the critical value of damage variable is used to decide the macroscopic crack growth. However, one of emerging issues of CDM is how the macroscopic crack can be defined, because it is difficult to decide on the critical value. In addition, when cracks are closed or opened by external force, the material state of the cracked element depends on the crack conditions. Therefore, the frictional sliding of macroscopic crack is important to explain shear localization phenomena by compressive force, contact effect of the cracked element should be considered when the fracture is subjected to compressive and shear stress fields. So, an Element Partition Method (EPM) is proposed to describe the contact and friction effect of fracture faces.

Damage mechanics

CDM is based on the micro- and macro-processes of nonlinear mechanical behavior. In a microscopic view, breaking of atomic bonds causes material damage and cracks initiate. Depending on the type of damage, scalar D, vector $\mathbf{D}$ or tensor (D_{ij}, D_{ijkl}) variables are used to describe damage. Damage vectors and tensors have been introduced to take into account anisotropic stiffness degradation. Currently, in our damage model, a single scalar damage variable is used because our material is considered isotropic.

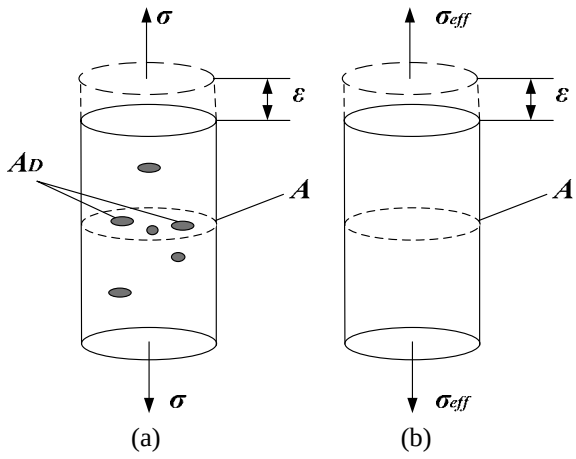

Fig. 13 (a) Schematic of damaged area and the intersection surface, (b) Stress equivalence principle

In the damage model used here, the "effective stress" approach introduced by Rabotnov (1968) is used. If the damage is assumed to be isotropic, it has the same value in all directions, then the scalar damage variable D can be defined as:

$$D = \frac{A_D}{A} \tag{6}$$

where A is the intersection surface of specimen and A_D is the area of all microcracks on the intersection surface A in Fig 13(a). The "effective stress" is then defined using the axial stress and the damage variable as below:

$$\sigma^{eff} = \frac{\sigma}{1-D}, 0 \le D < 1 \tag{7}$$

The stress-strain relation for isotropic damage is obtained:

$$\sigma_{ij} = (1-D) C^e_{ijkl} \varepsilon^e_{kl} \tag{8}$$

In continuum damage mechanics (CDM), damage can be considered as a macroscopic state variable that affects stiffness degradation of the material.

$$E' = (1-D)E \tag{9}$$

Scalar type of damage parameter is obtained using the maximum principal strain $\varepsilon_1=\sigma_c/E$ for shear failure and the minimum principal strain, $\varepsilon_3=\sigma_t/E$, for tensile failure (T. Wong 2006).

$$D = 1-\frac{\lambda\sigma_c}{E\varepsilon_1} \tag{10}$$

for shear failure, where σ_c is the compressive strength of material and

$$D = 1-\frac{\lambda\sigma_t}{E\varepsilon_3} \tag{11}$$

for tensile failure, where σ_t is the compressive strength of material.

In order to test the three-dimensional damage-based crack propagation algorithm, several factors such as stress regime, rock type, heterogeneity, and internal frictional sliding are carefully considered. At this stage of the work, only mechanical behavior of rock is simulated, thermo-hydro-mechanically coupled processes of rock formation and fracture will be developed in the next steps.

Fracture growth in uniaxial compression

Rock fracturing patterns from various experiments reported by Akharajanthachot et al are shown in Fig. 14 (B. Akharajanthachot 2009). The fracturing pattern is complex and it is challenging to replicate these fracturing patterns using numerical methods. However, the most common pattern of the fractured rock specimen is shear faulting phenomena during triaxial compression. The shear faulting phenomena depends on many parameters such as strength, heterogeneity, initial flaws, composition pattern, grain size of rock, etc.

Simulation of faulting in uniaxial compression using the combined EPM-Damage model (Fig 15) shows a pattern similar to a number of experimental results in Fig. 14. Especially, shear faulting phenomena is observed in both simulation and experiments. However, there are differences that are caused by the limitations of numerical simulation to replicate a real material. Heterogeneity, microcracks, and grain size could affect on strength distribution in a brittle rock. Rather than attempting to consider grain size in numerical simulations, a probability distribution function is used to characterize the strength of fine and coarse grained rock in this study. Strength heterogeneity of brittle rock is characterized by Weibull distribution function (Weibull 1951). The Weibull distribution function was chosen due to its flexibility. Random values generated by Weibull distribution function are applied to both stiffness and compressive strength to represent heterogeneous character of rock. Average value of stiffness is 73.5GPa, so that stiffness is distributed to each element by random variables. Weibull distribution parameters *m=1, a=5* for stiffness distribution and *m=1, a=4* for compressive strength distribution are used to characterize rock heterogeneity of the 3D specimen.

$$f(m) = \frac{a}{m_0}\left(\frac{m}{m_0}\right)^{a-1}\exp\left[-\left(\frac{m}{m_0}\right)^{a}\right] \tag{12}$$

where m_0 is a scale parameter which is proportional to the mean value of the random variable, the parameter a determines the shape of the distribution function. In Table. 2, material and model parameters are shown, which is used in this simulation.

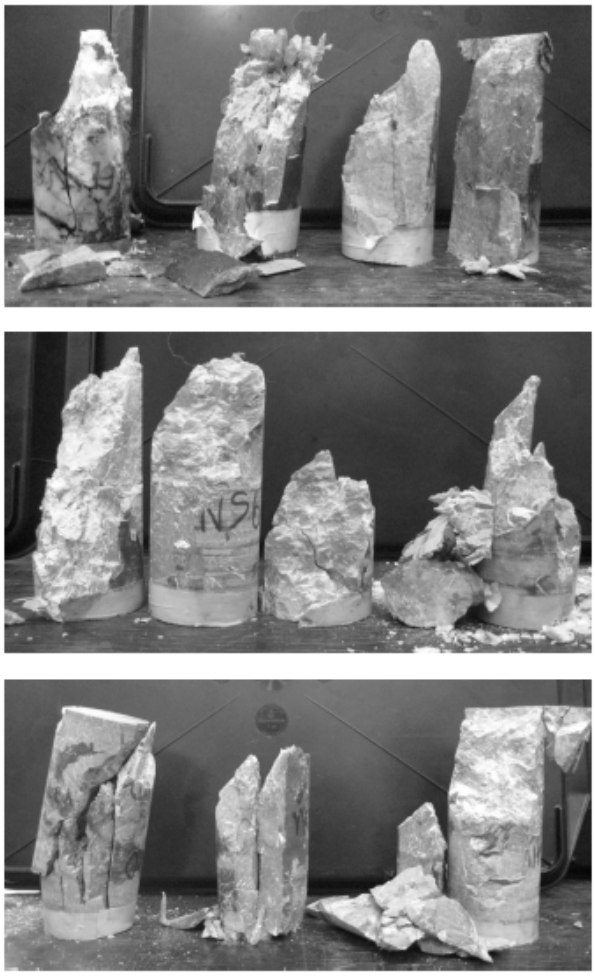

Fig. 14 The post-test specimens of uniaxial compression test by Akharajanthachot et al. (B. Akharajanthachot 2009).

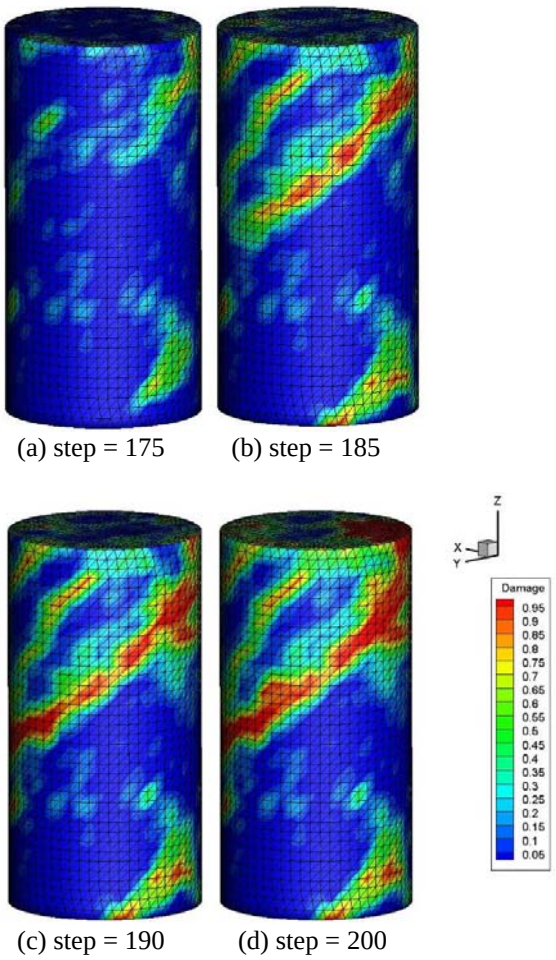

(a) step = 175 (b) step = 185

(c) step = 190 (d) step = 200

Fig. 15 Damage propagation along steps.

The incremental displacement is $\Delta d=3.55\times10^{-3}mm$. Crack was initiated at step 175 and applied displacement on top surface is *d=6.21E-01mm* and then fully ruptured fracturing occurs in a very short period, because rock is very brittle material. Also, broad and spotted damage propagation is observed due to the material heterogeneity in Fig. 16.

Table 2: Simulation parameters for uniaxial compression test.

Young's Modulus	73.5 GPa
Poisson ratio	0.25
Num. of elements	57,153
Num. of nodes	11,015
Critical stress	50 MPa
Dimension of specimen	*H=2m r=0.5m*
Weibull distribution parameters	m=1, a=5 m=1, a=4
Incremental Δd	$3.55\times10^{-3}mm$

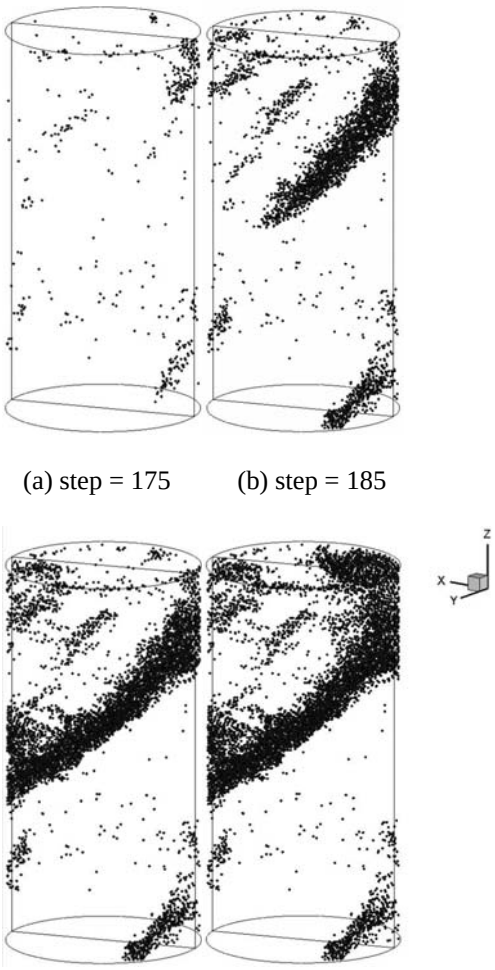

(a) step = 175 (b) step = 185

(c) step = 190 (d) step = 200

Fig. 16 Scatter of fracture propagation along steps.

Table 3: Simulation parameters for embedded crack growth.

Young's Modulus	73.5 GPa
Poisson ratio	0.25
Inclination angle	45°
Shape of crack	Circular
Radius of crack	*0.02 m*
Num. of element	142,480
Num. of nodes	26,597
Critical stress	50 MPa
Dimension of specimen	*0.1m×0.1m×0.3m*
Incremental Δd	$3.55\times10^{-5}mm$

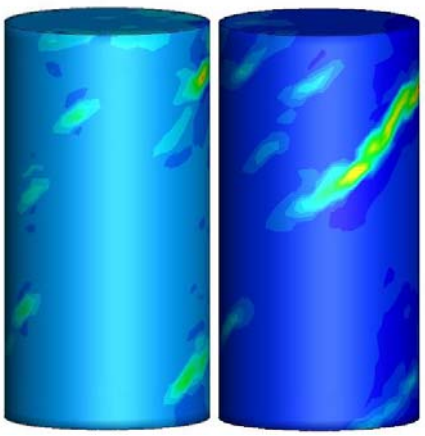

(a) step = 175 (b) step = 185

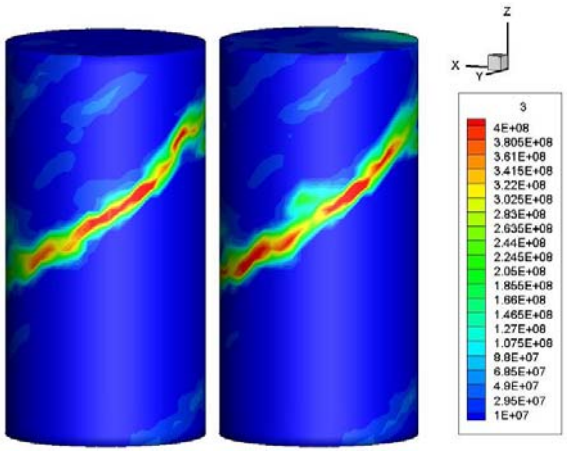

(c) step = 190 (d) step = 200

*Fig. 17 Principal stress (*Pa*) propagation along steps.*

Mixed-mode crack growth in rectangular specimen

Three-dimensional crack growth in uniaxial compression from an initially embedded circular crack has been developed in this section. The extension of secondary cracks in a brittle rock under slow uniaxial compression was shown. Secondary cracks are growing parallel to uniaxial compression due to transverse shear localization. Forces are originated from sliding of upper and lower of contact area and the shear friction force leads growth of secondary cracks (wing crack) in opposite side of primary crack. In reality, 3D crack growth mechanism is more complicated. While secondary crack growth in opposite side of the contact surface (pre-existing crack) is observed in Mode II condition, the initial crack could also grow in the lateral direction due to Mode III condition. The numerical simulations show significant difference between 2D case and 3D case. While a 2D single pre-existing crack can grow significantly in the direction of compression, the 3D pre-existing crack does not grow sufficiently long branching cracks because crack grows to laterally in Mode III. In Fig. 19 (b), shear slip fault continuously grew in the lateral direction of the initial crack surface. Parameters used for numerical domain are shown in Table 3. The sampel size is *0.1m×0.1m×0.3m* and radius of initially embedded circular crack is *0.02m*; inclination of pre-existing crack is 45°. The incremental displacement is $\Delta d=3.55\times10^{-5}$mm for each step and total step is 800.

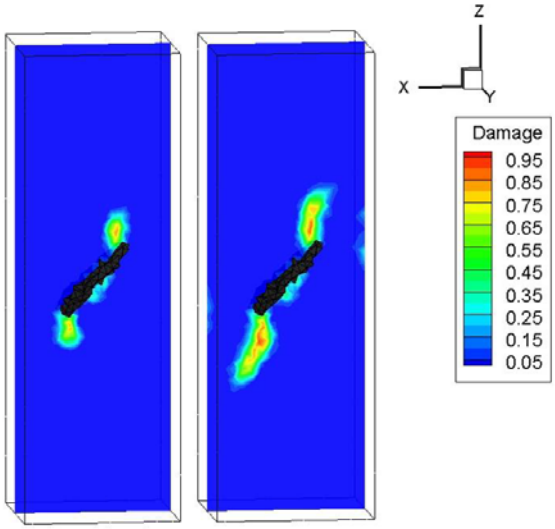

(a) step = 730 (b) step = 780

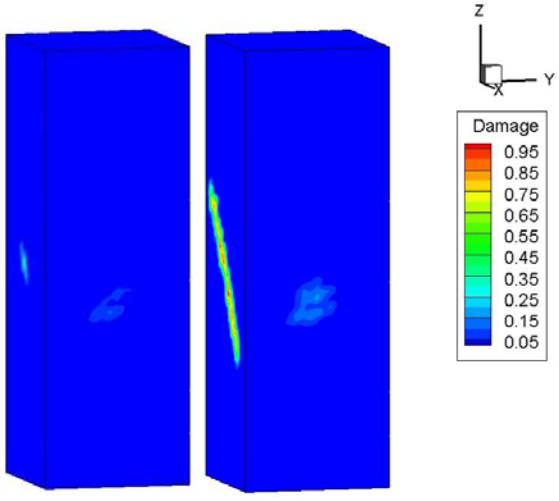

(c) step = 730 (d) step = 780

*Fig. 18 Intersection view of damage parameter propagation in x-z plane (y=0.05*m*).*

In Fig. 19(c-d), secondary crack wing grows parallel to the major compression, since shear forces are act on both upper and lower part of pre-existing crack. However, secondary crack grows in the lateral direction of pre-existing crack and meets the free surface. Fig. 18 (a-b) show wing crack has initially grown in the major compression direction; however the direction changes due to the presence of the free surface of the 3D specimen. In 2D case, since there is no Mode III fracture, the secondary crack could grow continuously toward the compression direction, but a 3D secondary crack growth from pre-existing circular crack occurs in mixed Mode II & Mode III, so that 3D fracture propagation becomes more complicated.

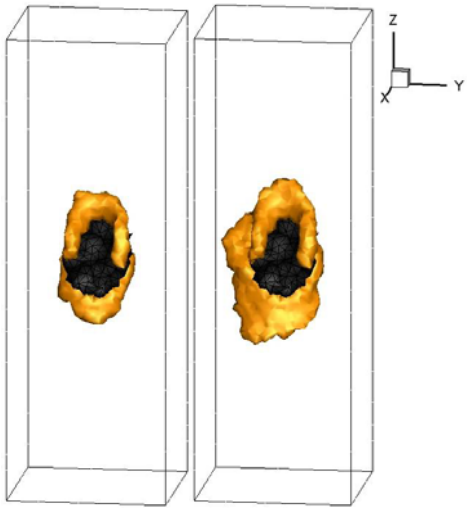

(a) step = 730 (b) step = 780

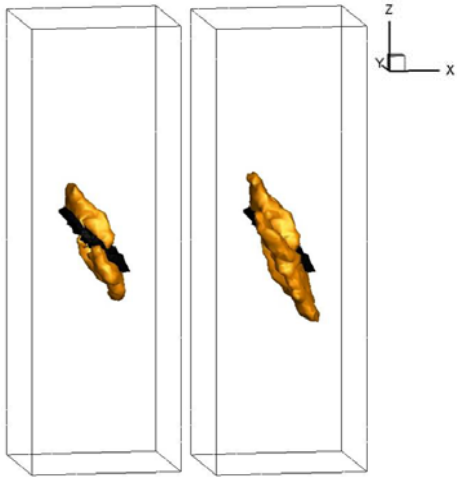

(c) step = 730 (d) step = 780

Fig. 19 Front view and side view of 3D crack growth using iso-surface.

CONCLUSION REMARKS

Numerical simulation of 3D fracture propagation in brittle rock is studied using two numerical approaches. One approach uses the virtual multidimensional bonds evolution function in micro scale (VMIB). It is found that the typical features of 3D tensile and compressive fracture propagation could be represented. Especially, simulation results by 3D VMIB and 3D EPM show the propagation of Mode III fracture. Such simulations improve understanding of 3D fracture propagation mechanism and provide a means for designing multiple hydraulic fractures. The simulation results suggest that the methods are feasible for simulating 3D fracture. Furthermore, 3D simulation of multiple hydraulic fractures shows good agreement with results of theoretical analysis. As the pore pressure and thermal effects will be introduced into this model, it can be used to simulate other situations of interest. Another numerical approach to rock fracture modeling used the continuum damage mechanics with element partition methodology to simulate 3D crack growth. The combined 3D EPM-Damage model is also successfully simulates shear fracturing propagation by Mode II and Mode III. Simulation results of crack growth in compression are in qualitative agreement with experimental observations of 2D and 3D crack propagation in brittle materials. Work in underway to simulate larger scale problem using more realistic representation of rock properties.

ACKNOWLEDGEMENT

This project was supported by the U.S. Department of Energy Office of Energy Efficiency and Renewable Energy under Cooperative Agreement DE-PS36-08GO1896. This support does not constitute an endorsement by the U.S. Department of Energy of the views expressed in this publication.

REFERENCES

Adams, M., and Sines, G. (1978). "Crack extension from flaws in a brittle material subjected to compression." *Tectonophysics*, 79, 97-118.

B. Akharajanthachot, P. K. (2009). *Rock mechanics testing of Khao Soon Tungsten project, Nakorn Srithummarad*: Bureau of Primary Industries, Department of Primary Industries and Mines, Thailand.

Bobet, A., and Einstein, H. H. (1998). "Fracture Coalescence in Rock-type Materials under Uniaxial and Biaxial Compression." *International Journal of Rock Mechanics & Mining Sciences*, 35(7), 863-888.

Dyskin AV, S. E., Jewell RJ, Joer H, Ustinov KB. (2003). " Influence of shape and locations of initial 3-D cracks on their growth in uniaxial

compression." *Engineering Fracture Mechanics*, 70(15), 2115-2136.

Gao, H., and Klein, P. (1998). "Numerical Simulation of crack growth in an isotropic solid with randomized internal cohesive bonds." *Journal of Mechanics, Physics, Solids*, 46(2), 187-218.

Klein, P., and Gao, H. (1998). "Crack nucleation and growth as strain localization in a virtual-bond continuum." *Engineering Fracture Mechanics*, 61(1), 21-48.

Lazarus, V. (2003). "Brittle fracture and fatigue propagation paths of 3D plane cracks under uniform remote tensile loading. ." *International journal of Fracture*, 112(1-2), 23-46.

Lee, S. H., and Ghassemi, A. (2010). " Themo-poroelastic analysis of injection-induced rock deformation and damage evolution"*Stanford Geothermal Workshop*. City: Stanford University, CA.

Min, K. S., Zhang, Z., and Ghassemi, A. "Numerical Analysis of Multiple Fracture Propagation in Heterogeneous Rock induced by Hydraulic Fracturing." *Presented at the 44th US Rock Mechanics Symposium*, Salt Lake City.

T. Wong, R. H. C. W., K.T. Chau, C.A. Tang. (2006). "Microcrack statistics, Weibull distribution and micromechanical modeling of compressive failure in rock." *Mechanics of Materials*, 38(2006), 664-681.

Weibull, W. (1951). "A statistical distribution function of wide applicability." *Journal of Applied Mechanics*, 18, 293-7.

Zhang, Z. N., and Ge, X. R. (2005). "Micromechanical consideration of tensile crack behavior based on virtual internal bond in contrast to cohesive stress." *Theoretical and Applied Fracture Mechanics*, 42, 342-359.

Zhang, Z. N., and Ghassemi, A. (2010). "The Virtual Multidimensional Internal Bond Method for Simulating Fracture Propagation and Interaction in Poroelastic Rock." *International Journal of Rock Mechanics & Mining Sciences*, In progress.